

## Investigation of Fracture Parameters of V-Notches in a Polymer Material using Digital Image Correlation

Nasser Soltani <sup>1,\*</sup>, Mohammad Reza Yadegari Dehnavi <sup>2,\*</sup> & Iman Eshraghi <sup>3,\*</sup>

**Abstract:** In this study, digital image correlation method is employed to analyze displacement field around V-notches of a Polymethyl methacrylate (PMMA) element with tip cracks. Using data extracted from DIC analysis, first intensity factor is obtained by least square fitting of the displacement field data and relations among stress intensity factors and displacement parameters. Since main influencing factors on the stress field are opening angle, crack length, and depth of V-notch, effects of these parameters on results are investigated. Experimental results are compared with those obtained from finite element analysis and accuracy of results and sources of errors are studied.

**Keywords:** Digital Image Correlation; Stress Intensity Factor; V-Notch

### 1. Introduction

Determination of fracture parameters such as stress intensity factor or J integral is necessary for evaluating the strength and prediction of service life of engineering structures. Since analytical methods involve complicated calculations, non-contact and full-field measurement optics methods such as holographic interferometry, caustics, moiré interferometry and photoelasticity have been usually used for evaluation of fracture parameters [1, 2]. Among different techniques of full field displacement measurement, digital image correlation (DIC) method has gained considerable attention during recent years because of its simplicity [3-5]. This method has gained widespread use mainly because it does not require complicated optical equipment and in contrast to other optical methods it does not utilize the interference of light waves, analysis of fringe pattern and then phase-unwrapping [6]. Because of the mentioned convenience in using this method, many researchers applied this method to various problems such as high temperature measurement, dynamic fracture and submicron deformation measurement [7]. To apply this method, experimental displacement field data in the local crack tip region are compared with the data obtained from analytical solutions to determine fracture parameters. Since this localized selection of displacement field data suffers from presence of errors in the experimental data, it has been suggested that full field information may be used to eliminate these errors [8, 9].

---

<sup>1</sup> Professor Nasser Soltani, Ph.D.; [nsoltani@ut.ac.ir](mailto:nsoltani@ut.ac.ir)

<sup>2</sup> Ing. Mohammad Reza Yadegari Dehnavi, M.Sc.; [m.yadegari@ut.ac.ir](mailto:m.yadegari@ut.ac.ir)

<sup>3</sup> Iman Eshraghi, Ph.D. Student; [ieshraghi@ut.ac.ir](mailto:ieshraghi@ut.ac.ir)

\* Intelligence Based Experimental Mechanics Center, School of Mechanical Engineering, College of Engineering, University of Tehran, P.O.Box :4111 Tehran, Iran

In this study, displacement field obtained from DIC experiment have been used to determine stress intensity factors for mode I fracture problem of a PMMA sample. Linear least-squares approach is applied to obtain unknowns such as stress intensity factors and rigid body displacements and rotation. The effects of v-notch opening angles and depths in accordance with tip crack length are investigated and compared to those obtained by finite elements. Results show good agreement between two methods. The sources of error are identified and the effects of them on the results are discussed. It has been shown that in the absence of out-of-plane motion, this method can successfully be used to obtain stress intensity factors.

## 2. DIC basics and experimental setup

### 2.1. Fundamentals of Digital Image Correlation

In general, three steps are included in two-dimensional DIC method. The first step is the preparation of specimen and experimental system. For the second step digital images of the planar specimen surface before and after loading are captured and recorded. Utilizing a computer program for post processing of the acquired images to obtain displacement and strain field information concludes the final step of the method. To perform the first step, a random speckle-like black and white dot patterns are created on specimen surfaces. For the next step the camera is placed with its optical axis normal to the specimen surface, imaging the planar specimen surface in different loading states onto its sensor plane. The digitized images are compared and subsets are matched between one image and the other to finalize the required steps of performing a DIC technique. Depending on the choice of the loading and required accuracy, a subset may comprise several pixels. Then its location in the deformed image is found and thus its displacements are determined. A normalized cross-correlation coefficient,  $C$ , defined by Eq. (1) is used to improve the estimate of the displacements [5, 10].

$$C\left(x, y, u, v, \frac{\partial u}{\partial x}, \frac{\partial u}{\partial y}, \frac{\partial v}{\partial x}, \frac{\partial v}{\partial y}\right) = 1 - \frac{\sum G_r(x, y)G_d(x', y')}{\sqrt{\sum G_r(x, y)^2 G_d(x', y')^2}} \quad (1)$$

where  $u$  and  $v$  are the displacement components at the center of the subset,  $G_r$  and  $G_d$  are the grey levels of the reference and deformed images, respectively, and  $(x, y)$  and  $(x', y')$  are the coordinates of a point in the subset before and after deformation respectively.  $(x', y')$  is related to  $(x, y)$  by Eq. (2) as follows:

$$x' = x + u + \frac{\partial u}{\partial x} \Delta x + \frac{\partial u}{\partial y} \Delta y \quad ; \quad y' = y + v + \frac{\partial v}{\partial x} \Delta x + \frac{\partial v}{\partial y} \Delta y, \quad (2)$$

in which  $\Delta x$  and  $\Delta y$  are distances from the subset center to the point  $(x, y)$  in the  $x$  and  $y$  directions respectively (Fig. 1). Since the correlation coefficient  $C$  is a function of the displacement and displacement gradients components, these components are determined by looking for a set of the displacements and a set of displacement gradients that minimize this correlation coefficient. Displacements in

Eq. (2) can take sub-pixel values, thus an interpolation scheme must be employed to determine the intensity values at sub-pixel locations. Two major interpolation schemes are bilinear and bicubic interpolations [7].

The process of searching for unknown displacement and displacement gradients components begins with a rough estimate of displacement components and setting displacement gradients equal to zero. At the end of this step the displacements are found with an accuracy of 1 pixel. Newton-Raphson method is then used to find displacement gradients and displacement components with sub-pixel accuracy. The results of previous step are considered as the initial values for the Newton-Raphson method. More details can be found in the works by Bruck et al. [5] and Lu and Cary [11].

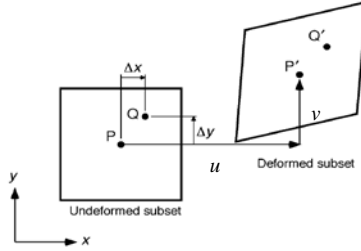


Fig. 1. Undeformed and deformed subsets [6]

## 2.2. Estimation of Stress Intensity Factor

For a displacement data point, considering mode I and II loading of cracks in plane problem and taking into account in-plane rigid body displacements and rigid body rotation, the displacement components around a crack tip are expressed as:

$$u_j = \sum_{n=1}^{\infty} \frac{r_j^2}{2\mu} \left\{ a_n \left[ \left( \kappa + \frac{n}{2} + (-1)^n \right) \cos \frac{n}{2} \theta_j - \frac{n}{2} \cos \left( \frac{n}{2} - 2 \right) \theta_j \right] - b_n \left[ \left( \kappa + \frac{n}{2} - (-1)^n \right) \sin \frac{n}{2} \theta_j - \frac{n}{2} \sin \left( \frac{n}{2} - 2 \right) \theta_j \right] \right\} + u_0 - \varphi r_j \sin \theta_j \quad (3)$$

$$v_j = \sum_{n=1}^{\infty} \frac{r_j^2}{2\mu} \left\{ a_n \left[ \left( \kappa - \frac{n}{2} - (-1)^n \right) \sin \frac{n}{2} \theta_j + \frac{n}{2} \sin \left( \frac{n}{2} - 2 \right) \theta_j \right] + b_n \left[ \left( \kappa - \frac{n}{2} + (-1)^n \right) \cos \frac{n}{2} \theta_j + \frac{n}{2} \cos \left( \frac{n}{2} - 2 \right) \theta_j \right] \right\} + v_0 + \varphi r_j \cos \theta_j$$

the Subscript  $j$  denotes the  $j$ th data point with the coordinate  $(x_j, y_j)$  of  $M$  total data points.  $u_j$  and  $v_j$  are the displacement components in  $x$  and  $y$  directions respectively,  $\mu$  is the shear modulus, and  $\kappa$  is  $(3-\nu)/(1+\nu)$  for plane stress and  $3-4\nu$  for plane strain.  $u_0$  and  $v_0$  are the rigid body displacement components and

$\varphi$  is the rigid body rotation angle in radians. Polar coordinates of a point relative to the crack tip location,  $(r_j, \theta_j)$ , are related to Cartesian coordinates,  $(x_j, y_j)$ , by (Fig. 2):

$$r_j = \sqrt{(x_j - x_0)^2 + (y_j - y_0)^2} \quad ; \quad \theta_j = \tan^{-1} \left( \frac{y_j - y_0}{x_j - x_0} \right). \quad (4)$$

where  $(x_0, y_0)$  is the coordinates of crack tip location.

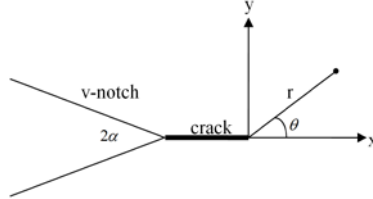


**Fig. 2.** Cartesian and polar coordinates at the crack tip of a v-notch

First and second intensity factors ( $K_I, K_{II}$ ) are given by Eq. (5) as:

$$K_I = \sqrt{2\pi} a_1 \quad ; \quad K_{II} = -\sqrt{2\pi} b_1 \quad (5)$$

Here only mode I loading is considered and linear least square fitting will be used to evaluate unknowns  $K_I, u_0, v_0$ , and  $\varphi$ .

### 2.3. Specimens and Test Setup

Polymethylmethacrylate (PMMA) is used as the test material. Elasticity modulus,  $E$ , and Poisson's ratio,  $\nu$ , of the material were measured to be as  $E=3.33 \text{ GPa}$  and  $\nu = 0.33$  respectively. The specimen and the experimental setup are shown in Fig. 3.



**Fig. 3.** Experimental setup

The width of the specimen is 50 mm and its thickness is equal to 4 mm. DIC tests were performed for two different notch angles of magnitude  $2\alpha = 30^\circ, 120^\circ$ . For

each angle four values of v-notch depth, i.e. 5, 8, 11, and 14 mm, are considered. For constant angle and depth of a v-notch, the length of tip crack is varied from 3 to 12mm in a 3mm increment. For the purpose of determining the magnification factor and subset size, rigid body translation tests were performed. The magnitude of the applied axial force was varied from 0 to 70kgf with an increment of 3.5 kgf. Random patterns on the specimen surface were recorded by a charged-coupled device (CCD) camera (Art-Cam 320p equipped with a Fujian 55 mm lens) as shown in Fig. 3. The images were captured with a spatial resolution of  $2288 \times 1700$  pixels. The setup was settled on a vibration isolated table in order to eliminate noises. Each 1 mm of real distance corresponds to 20.41 pixels in the scaled images used for analysis.

### 3. Finite Element Modeling

For the purpose of comparison a finite element model has been created for analyzing the stress intensity factor of the specimen under given applied load. Figure 4 shows the FE model and type of mesh used in the vicinity of the crack tip. Because of symmetry, only half of the specimen has been modeled with symmetric boundary conditions applied on the lower line of the model. Five contours were taken around crack tip for estimation of the crack intensity factor. Deformation of the model after applying the tensile load in combination with the crack opening is shown in Fig. 4

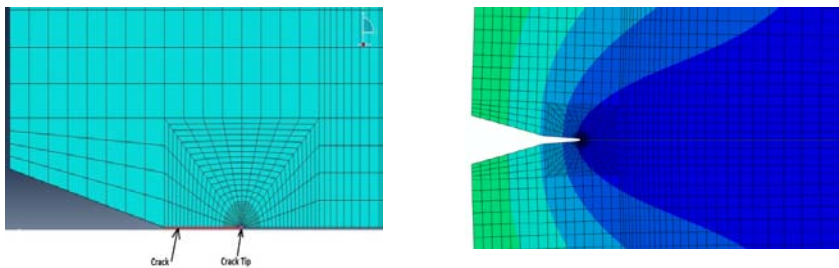
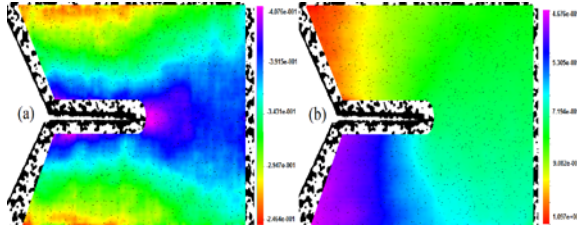


Fig. 4. The mesh around the crack (left) and opening of the crack after loading (right)

### 4. Results and Discussion

Results of displacement fields obtained from a DIC analysis of a specimen with a  $30^\circ$  v-notch angle are shown in Fig. 5. 50 data points are extracted from the obtained displacement fields to perform a least square fitting for determining the stress intensity factor. The magnitude of the standard error and correlation coefficient (for least square fitting) are equal to  $3e-7$  and 0.97 respectively for the applied load of 70 kgf. The magnitude of obtained stress intensity factor from DIC analysis and FE modeling for various loads and various v-notch angles are given in Fig. 6 (a) and (b). These figures show good agreement between the results of finite element analysis and DIC results. As it may be observed the magnitude of v-notch angle has small effect on the values of stress intensity factor. Also it may be noticed that the percentage of the error for experimental data decreases with increase of the applied load. This is mainly because higher axial loads produce greater displacements which will result in relatively smaller errors in estimation of the displacement fields during DIC post processing. The linear variation of first intensity factor with the applied

load is also clear from the given figures for both of FE and DIC results for all v-notch angles.



**Fig. 5.** Displacement field obtained from DIC experiment: (a) displacement field in x direction (b) displacement field in y direction

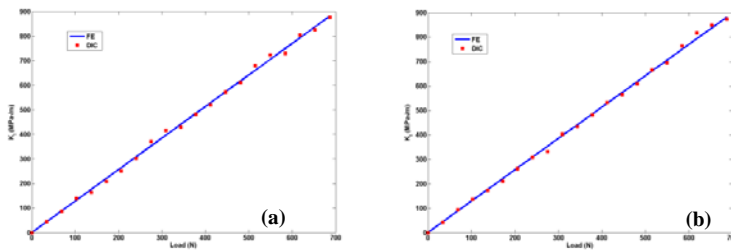


**Fig. 6.** Variation of first intensity factor with the applied load for various v-notch angles and obtained from finite element and DIC analysis (a)  $2\alpha = 30^\circ$  (b)  $2\alpha = 120^\circ$

Tables 1 and 2 compare first intensity factors obtained from DIC analysis and finite element simulation for a constant load of 20 kgf. Good agreement is shown to exist between two methods.

**Table 1. First intensity factor for different tip crack lengths and angles of 5 mm depth v-notches**

V-Notch Angle (Degree)	Tip Crack Length (mm)	First Intensity Factor ( $MPa\sqrt{m}$ )	
		DIC	FEA
30	6	0.23021	0.22253
	12	0.32505	0.31624
120	6	0.19969	0.20146
	12	0.33014	0.34759

As it could be seen in Table 1, for constant v-notch depth and angle values, increase of tip crack length leads to the increase in first intensity factor. However it may be observed that the difference of first intensity factor values for different v-notch angles is high for small tip crack lengths and this difference is gradually attenuated for higher tip crack lengths. Also it may be noticed from Table 2 that, as it may be expected, first intensity factor increases for both increasing the tip crack length and v-notch depth in the case of a constant v-notch angle.

**Table 2. First intensity factor for different tip crack lengths and depths of 30° v-notches**

V-Notch Depth (mm)	Tip Crack Length (mm)	First Intensity Factor ( $MPa\sqrt{m}$ )	
		DIC	FEA
8	3	0.23705	0.22952
	9	0.35760	0.32698
14	3	0.26233	0.24649
	9	0.36549	0.35198

Variation of first intensity factor with v-notch depth and tip crack length for a 120° v-notch is shown in Fig. 7. As it may be observed first intensity factor increases with both increase in v-notch depth and tip crack length. Although the rate of increase of first intensity factor values is higher when the crack length increases.

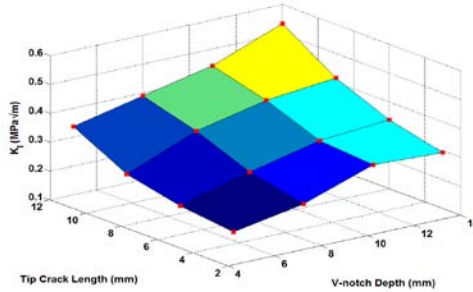


**Fig. 7.** First intensity factor of a 120° v-notch vs. its depth and tip crack length

Variation of first intensity factor with v-notch depth for 6 and 9mm tip crack lengths for 30° and 120° v-notch angles are compared in Fig. 8 (a) and 8(b) respectively. It is clear that first intensity factor for all values of v-notch depth is always higher for 30° v-notch. The difference between first intensity factors for two v-notch angles is high for lower v-notch depths and this difference decreases for higher values of v-notch depth.

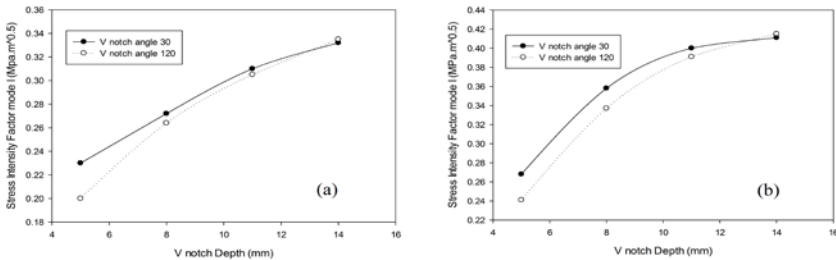


**Fig. 8.** Variation of first intensity factor with the v-notch depth for (a) 6 mm and (b) 9 mm length tip crack

## 5. Conclusions

An experimental study was performed to determine first stress intensity factor of a PMMA specimen under mode-I loading condition. Results of DIC analysis were compared to those given by finite element analysis and excellent agreement was shown to exist. It was also shown that the v-notch angle has small effect on the value of first intensity factor when the length of crack is held constant in large tip crack length. It was also demonstrated that in the case of a v-notch with a tip crack within the elastic region and for mode-I loading conditions, the relation between first intensity factor and applied tensile load is linear. The dependency of first intensity factor on v-notch depth and tip crack length was also studied and an increasing behavior was shown to exist. This behavior, however, is not the case for variation of v-notch angle and while for small values of tip crack length first intensity factor decreases by increasing v-notch angle, for larger values of tip crack length, the difference is almost negligible. The method adopted in this study can be fully developed to take into account the effects of mode-II loading condition for determination of combined first and second intensity factors.

## References

- [1] Smith C. W. and Kobayashi A. S., "Experimental fracture mechanics," in *Handbook on Experimental Mechanics*, Kobayashi A. S., ed. (VCH, New York, 1993), pp. 905-968.
- [2] Chiang F., "Moire' and speckle methods applied to elastic-plastic fracture studies." in *Experimental Techniques in Fracture Mechanics*, Epstein J. S., ed. (VCH, New York, 1993), pp. 291-325.
- [3] Peters W. H. and Ranson W. F., "Digital imaging technique in experimental stress analysis," *Optical Engineering*, **21**, pp. 427-431(1982).
- [4] Sutton M. A, Wolters W. J., Peters W. H., Ranson W. F. and McNeill S. R., "Determination of displacements using an improved digital correlation method," *Image and Vision Computing*, **1**, pp. 133-139 (1983).
- [5] Bruck H. A., McNeill S. R., Sutton M. A. and Peters W.H., "Digital image correlation using Newton-Raphson method of partial differential correlation," *Experimental Mechanics*, **29**, pp. 261-268 (1989).
- [6] Yoneyama S., Morimoto Y., and Takashi M., "Automatic evaluation of mixed-mode stress intensity factors utilizing digital image correlation," *Strain*, **42**, pp. 21-29 (2006).
- [7] Vendroux G. and Knauss W. G., "Submicron deformation field measurements: part 2. Improved digital image correlation," *Experimental Mechanics*, **38**, pp. 86-92 (1998).
- [8] McNeill S. R., Peters W. H., and Sutton M. A., "Estimation of stress intensity factor by digital image correlation," *Engineering Fracture Mechanics*, **28**, pp. 101-112 (1987).
- [9] Andanto-Bueno J. and Lambros J., "Investigation of crack growth in functionally graded materials using digital image correlation," *Engineering Fracture Mechanics*, **69**, pp 1695-1711 (2002).
- [10] Sutton M. A., McNeill S. R., Helem J. D. and Chao Y-J. "Advances in two- and three-dimensional computer vision". in: *Photomechanics*, Rastogi P. K., ed. (Springer, Berlin, 2000), pp. 323-372.
- [11] Lu H. M. and Cary P. D., "Deformation measurements by digital image correlation: implementation of a second-order displacement gradient," *Journal of Experimental Mechanics*, **40**, pp 393-400 (2000).